Desalination and Water Treatment
www.deswater.com
doi: 10.5004/dwt.2021.27477

231 (2021) 229–243
August

Removal of Hg(II) ions with CD/DVD waste-derived aminated polycarbonate: adsorption and optimization studies

Saidu Akun Abdallah[a,b], Kheng Soo Tay[a,*], Kah Hin Low[a,*]

[a]*Department of Chemistry, Faculty of Science, Universiti Malaya, Kuala Lumpur 50603, Malaysia, emails: khengsoo@um.edu.my (K.S. Tay), lowkayin@um.edu.my (K.H. Low), asabayu@yahoo.com (S.A. Abdallah)*
[b]*Department of Science Laboratory Technology, College of Science and Technology, Hussaini Adamu Federal Polytechnic, P.M.B. 5004, Kazaure, Jigawa, Nigeria*

Received 4 January 2021; Accepted 30 May 2021

ABSTRACT

A massive quantity of plastic waste is generated daily, leading to serious environmental issues. As one of the plastic wastes, the waste optical discs contain polycarbonates that can be recovered and utilized as value-added materials. In this work, polycarbonate was recovered from waste discs and aminated. The adsorption of aqueous Hg(II) ions onto the aminated PC was investigated, where the experimental variables were evaluated with a Box–Behnken design. The response surface model revealed that 1 mg L^{-1} of initial Hg(II) ions concentration, pH 7, and 10 min contact time as the optimal settings for mercury removal. According to the validation study on spiked samples, the mercury removal efficiency was ranged from 97% to 99%, which is consistent with the model prediction and considerably independent from the effect of sample matrices under the experimental conditions of this work. Regarding the best fitting among the investigated adsorption models, the adsorption process is well-described by the Freundlich isotherm, which indicated monolayer adsorption. The adsorption process was also found to follow the pseudo-second-order kinetic model that described the chemisorption. The result of this study suggested that the waste-derived aminated polycarbonate could be a potential adsorbent for the treatment of mercury in contaminated water.

Keywords: E-waste; Experimental design; Mercury; Plastic; Water treatment

1. Introduction

The rate of global consumption of plastics is at an alarming level due to population growth and resulting in producing large quantities of plastic wastes, which causes plastic pollution [1]. Compact discs (CDs) and digital video discs (DVDs) containing about 95% polycarbonate (PC) have been part of the plastic wastes [2]. CDs and DVDs were manufactured to support the information technology sector; however, due to the evolution of more advanced data storage facilities, the demand for optical discs is drastically faded. Subsequently, vast quantities of CDs and DVDs were discarded in landfills. Disposal of optical discs that contain a large portion of PC in landfills is not a good option. The monomer of PC, bisphenol A, an endocrine disruptor, is leachable into the environment, and it could be a concern of pollution [3]. Therefore, there is a critical need to reduce the disposal of CDs and DVDs.

Several approaches and strategies for upcycling CD/DVD wastes have been proposed. However, there are still noticeable weaknesses. For example, the attempt to transform waste optical discs into activated carbons requires a long duration of pyrolysis [4]. Similarly, waste CDs also have been charred into a reducing agent to serve the mineral iron processing [5]. The preparation of such carbonaceous products generally involves high thermal energy (550°C–1,550°C), and it produces hazardous gases. Although chemical recycling through glycolysis, alcoholysis, aminolysis, and digestion has also been reported, hazardous bisphenol A is still an inevitable by-product [6]. So far, the above

* Corresponding authors.

options generally suffer certain drawbacks and are rather sub-optimal for practical applications. This study, therefore, was motivated to explore economic innovation that aims to convert PC wastes into useful material.

Polymeric materials have emerged as potential alternatives for removing pollutants via adsorption, and this research area has remained the focus of many studies [7,8]. For instance, reactive functionalized polymeric (ion-exchange) resins that demonstrate attractive features for speed pollutant trapping are used extensively in water treatment due to better surface contact in an aqueous medium [9]. Although PC might not display excellent adsorption affinity in contaminant removal, it contains functional groups such as aromatic rings and polyester, which could be altered chemically [10] to enhance its affinity towards contaminants [7]. According to literature reports, aminated materials are sensible adsorbent candidates against Hg(II) ions due to the binding preference between Hg(II) ions and the nitrogen atom in the amine group [11].

Heavy metal pollution poses a serious concern to living organisms. Some of the heavy metals pollutants of great environmental concern include cadmium, lead, chromium, zinc, copper, and mercury. When ingested, some heavy metals can bioaccumulate in living organisms and result in serious ailments, including cancer, nervous system damage, and eventually death [12]. Mercury is considered one of the most poisonous metals. It is also persistent and bioaccumulative in both the food chain and human organs [13]. It is produced by anthropogenic activities such as mining, fossil fuel combustion, the manufacturing of mercury-containing products, etc. [7]. In the context of wastewater remediation, several technologies have been researched and applied. These technologies include ion exchange, coagulation, phytoremediation, osmosis, photo-catalysis, and adsorption [12,14–16]. Among these technologies, adsorption is the most versatile, well-researched, and natural process used for wastewater remediation because of its simplicity and economic feasibility [17–19]. To date, various adsorbents for environmental remediation have been synthesized and studied by many researchers [7]. Still, the search for cost-effective adsorbents is a continuous process since the cost is an essential parameter in the adsorption process [20].

This work, therefore, aims to explore the feasibility of utilizing waste optical discs as a resource in the fabrication of adsorbent to treat Hg(II) ions in aqueous matrices. The attempt includes purification of PC from CD/DVD waste, functionalization with the amine moiety, and subsequent adsorption studies. The adsorption behavior of Hg(II) ions was investigated at various experimental conditions using response surface methodology (RSM), where the influence factors, that is, the initial concentration of the Hg(II) ions (IC), pH, and contact time (CT) were optimized within the practical range. Contrary to the conventional one factor at a time method, RSM assesses the effects and interactions of multiple factors simultaneously, hence, providing a better understanding of the experimental variables at reducing time and cost [21,22]. The adsorption isotherms and kinetics of Hg(II) ions adsorption onto the aminated PC were also investigated. To the best of our knowledge, the potential of waste-derived aminated PC as an adsorbent has not been reported.

2. Methodology

2.1. Chemical reagents

All the chemicals used were of analytical grade. Hydrochloric acid, nitric acid, disodium hydrogen phosphate, sodium dihydrogen phosphate, hexamethylenediamine (HMDA), ethanol, methanol, dichloromethane were purchased from Merck (Germany). Hg(II) standard solution 1,000 mg L^{-1} was obtained from Sigma Aldrich (USA). All solutions were prepared using ultrapure water (UPW) produced from the ELGA water purification system. Various concentrations of the working standard solutions were prepared by diluting the stock solution using UPW. The pH of the solution was adjusted using the phosphate buffer.

2.2. Recovering polycarbonate from waste optical discs

The coating and label on the surface of the waste optical discs were first removed mechanically. The cleaned discs were then cut into small pieces and washed sequentially with 10% acetic acid solution, 5% sodium hydroxide solution, UPW, and dried at 80°C for ~12 h. The PC was purified by dissolving 1 g cleaned discs in 20 mL dichloromethane. The obtained solution was then filtered into 30 mL of methanol to precipitate the recovered polycarbonate (RPC). The collected RPC was thoroughly washed with UPW, dried at 80°C for ~12 h, sieved, and stored under a desiccator [23].

2.3. Amination of the recovered polycarbonate

The RPC was subjected to the amination reaction at room temperature (30°C ± 1°C), as reported by Delinder et al. [24] with little modification. 1 g of RPC was first suspended in 20 mL of various concentrations of HMDA ranging from 1 to 3 wt% in water in tightly sealed 50 mL glass vials. The vials were shaken using an orbital shaker at 50 rpm for ~12 h. After that, the suspensions were allowed to incubate for 48 h to ensure reasonable amination on the RPC substrate. The aminated RPC (ARPC) was washed with ultrapure water to remove excess HMDA, and the resultant ARPC was vacuum-dried, sieved, and stored in a desiccator before being used.

2.4. Characterization studies

The polymer samples were subjected to the following characterization and analysis: chemical functionality was evaluated by an attenuated total reflectance-Fourier transform infrared (ATR-FTIR) spectrometer (Perkin Elmer Spectrum 400, USA) for wavenumbers within 450–4,500 cm^{-1}; thermal behavior was investigated by using a simultaneous thermal analyzer (Perkin Elmer STA 6000, USA); surface morphology and elemental composition were examined using field emission scanning electron microscopy (FESEM, Hitachi SU8200, Japan) and energy-dispersive X-ray spectroscopy (EDX); The surface-specific area and porosity were analyzed using Brunauer–Emmet–Teller (BET) and Barrett–Joyner–Halenda (BJH) methods using an accelerated surface area and porosimetry system (Micromeritics ASAP 2020, USA); concentration of Hg(II) ions was

determined using a reducing vaporization mercury analyzer (Nippon Instruments Corporation RA-3, Japan).

2.5. Response surface methodology

Box–Behnken design (BBD), which is one of the response surface designs, was employed to explore the effect of experimental variables on Hg(II) adsorption removal. The targeted factors, including initial Hg(II) ions concentration (IC), solution pH, and contact time (CT), were investigated within the practical range at low (–1), middle (0), and high (+1) levels as presented in Table 1.

The design matrix was generated and analyzed using JMP 12.2 (SAS), where the following second-order polynomial model was postulated (Eq. (1)):

$$y = b_0 + \sum_{i=1}^{k} b_i x_i + \sum_{i=1}^{k} b_{ii} x_i^2 + \sum_{i=1}^{k} \sum_{j=i}^{k} b_{ij} x_i x_j + e \quad (1)$$

where y represents the response (percent Hg(II) ions removal), b_i is the main effect, b_{ii} is the quadratic effect, b_{ij} is the two-way interaction, and e is the random error [25]. The details can be found in Table S1. The fit of the regression model was assessed by the coefficient of determination (R^2), adjusted R^2, root mean square error (RMSE), and analysis of variance (ANOVA), Student's t-test as practiced elsewhere [26–28].

2.6. Adsorption experiments

The adsorption data was collected via batch adsorption experiments. Based on the preliminary test, the 250 μm-sieved ARPC demonstrated the highest removal efficiency as compared to those 300 and 600 μm (Fig. S1). The adsorption experiment was therefore conducted according to the designed treatments using 250 μm-sieved adsorbents in 25 mL of the respective Hg(II) ions solutions under sealed vials. Briefly, the mixtures were shaken at 150 rpm with an orbital shaker, and the residual concentration of Hg(II) ions were recorded at desired contact time. The percent Hg(II) ions removal (y) was calculated using Eq. (2) [17]:

$$y = \frac{C_0 - C_t}{C_0} \times 100\% \quad (2)$$

Table 1
Level of the selected parameters used in the BBD

Factors	Coded levels of parameters		
	–1	0	1
Initial Hg(II) ions concentration (mg L^{-1}) (x_1)	1	5.5	10
pH (x_2)	4	6	8
Time (min) (x_3)	10	50	90

where C_0 and C_t, represent the concentrations of Hg(II) ions (mg L^{-1}) at initial and at time t.

2.7. Adsorption isotherm studies

The adsorption equilibrium experiments were also conducted in batch mode, which consisted of individual mixtures of 50 mg of ARPC (250 μm) in 25 mL Hg(II) ions solution at the concentration ranging from 1 to 10 mg L^{-1}. The adsorption process was carried out at pH 7 and room temperature (30°C ± 1°C). The mixture was shaken using an orbital shaker at 150 rpm for 12 h. The supernatant was retrieved, and the equilibrium adsorbed Hg(II) ions per unit mass of ARPC was expressed as Eq. (3):

$$Q_e = \frac{C_0 - C_e}{m} \times V \quad (3)$$

where C_0 and C_e is the concentration of Hg(II) ions (mg L^{-1}) at equilibrium; m (g) is the amount of adsorbent, and V (L) is the volume of the aqueous solution. In order to investigate the adsorption behavior of Hg(II) ions on ARPC, the fitting of experimental data was attempted using the Langmuir, Freundlich, and Temkin isotherm models [21].

2.8. Adsorption kinetic studies

Batch adsorption, as described in the previous section, was adopted to illustrate the effect of contact time and the kinetic model. The data collected between 10 and 100 min were fitted to pseudo-first-order (PFO), pseudo-second-order (PSO), and intraparticle diffusion models [29].

2.9. Investigating the effect of real water matrix

The efficiency of ARPC for the removal of Hg(II) in real water samples was investigated using different water samples, including UPW, tap water, (TW) lake water (LW), mineral water (MW), and drinking water (DW). All the tests were performed in batch mode under the optimum settings. The supernatant was separated from the adsorbent, and the concentration of the remaining Hg(II) ions was evaluated.

2.10. Desorption and reusability study

To assess the economic viability of ARPC, four desorbing agents, including 0.75 M thiourea in 2% HCl, 1.5 M HNO_3, 1.5 M H_2SO_4, and 1.5 M HCl were employed to desorb the Hg(II) from the Hg(II)-loaded ARPC. Before each desorption test, the spent adsorbent was prewashed with UPW to remove any Hg(II) ion that was not adsorbed and allowed to dry under vacuum for 12 h. The percent Hg(II) ion recovery was calculated using Eq. (4) [30,31]:

$$\%\mathrm{Hg(II)}\ \text{recovery} = \left(\frac{\text{Amount of Hg(II) desorbed}}{\text{Amount of Hg(II) adsorbed}} \right) \times 100\% \quad (4)$$

The regeneration study was carried out using 0.75 M thiourea in 2% HCl because of its high regeneration ability. The adsorption–desorption process was carried out each cycle with fresh Hg(II) solutions [32]. The same process was repeated consecutively for four cycles.

3. Results and discussion

3.1. Characterization studies of the prepared adsorbents

The RPC reacted with the HMDA for ~60 h to produce the ARPC. The proposed reaction between the amine and the RPC is proceeding via nucleophilic substitution on the ester group O–(C=O)– of the PC with a chain scissoring to form a terminal hexylaminocarbamate. The proposed reaction is illustrated in Fig. 1.

The FTIR spectra of PC and ARPC are presented in Fig. 2. The peak at 1,766 cm^{-1} is attributed to carbonyl (C=O) of the ester group. The peaks at 1,216; 1,186; and 1,155 cm^{-1} represent the symmetrical and asymmetrical stretching vibrations of the ester groups of PC. Also, the peak observed at 1,503 cm^{-1} is attributed to the aromatic ring of PC [33]. Typically, the ARPC also shared the characteristic spectral peaks of the PC. The stretching vibration of the C–C bond of the phenyl group was observed at 1,598 cm^{-1} in the RPC [34]. This peak was replaced by two new peaks at 1,619 and 1,570 cm^{-1} attributed to the C–N vibration suggesting a successful amination reaction [35]. The intensity of these two peaks was found to increase with increasing HMDA loading on the ARPC.

The ARPC-Hg vibrational peak, on the other hand, depicted some variations from those of the ARPC. For instance, the peaks that attribute to the ester group were found to be shifted to 1,239; 1,212; and 1,173 cm^{-1}. Again, the aromatic ring vibration was shifted from 1,503 to 1,507 cm^{-1}. The peaks attributed to C–N ground were also found to be shifted from 1,619 and 1,570 cm^{-1} to 1,611 and 1,573 cm^{-1}. These changes could be attributed to the adsorbed Hg(II) ions onto the adsorbent.

The TGA as well as the derivative thermogravimetric (DTG) results of the polymers are presented in Fig. 3. A similar degradation pattern of the RPC [23] is depicted by ARPC 1% HMDA loading with an initial weight loss of ~79% occurring around 320°C to 531°C. The ARPC with 2% HMDA and ARPC with 3% HMDA loadings exhibited major degradation beginning at a much lower temperature (250°C–450°C) with a mass loss of about 74%. A second minor degradation occurring between 450°C and 700°C with about 16% weight loss was observed in all three polymers. The aminated polymers (ARPC) suffer a higher percentage of weight loss compared to the PC (81%) [34]. The observed mass losses might be related to the loss of volatiles in addition to the decomposition of the polymer matrix [35]. An increase in the HMDA % loading lowers the onset temperatures of the adsorbent. In other words, the presence of the HMDA lowers the decomposition temperatures of the polymers. This increase in weight loss confirms the successful amination of the RPC.

The FESEM images of surface morphology of RPC and ARPC are available in Fig. S2 and b. A significant variation was observed in the porous microstructures of these two materials. For RPC, the surface is covered with clusters of non-uniform micro-pores of RPC particles of various sizes; whereas the micrograph of the ARPC shows a rough surface covered by irregular shallow cavities. The difference in the morphological images reveals the changes in the surface property, which reflects the surface modification of RPC. At the same time, the EDX results (Table S2) confirmed the presence of nitrogen (N) in the aminated products as compared to RPC that contains carbon (C) and oxygen (O)

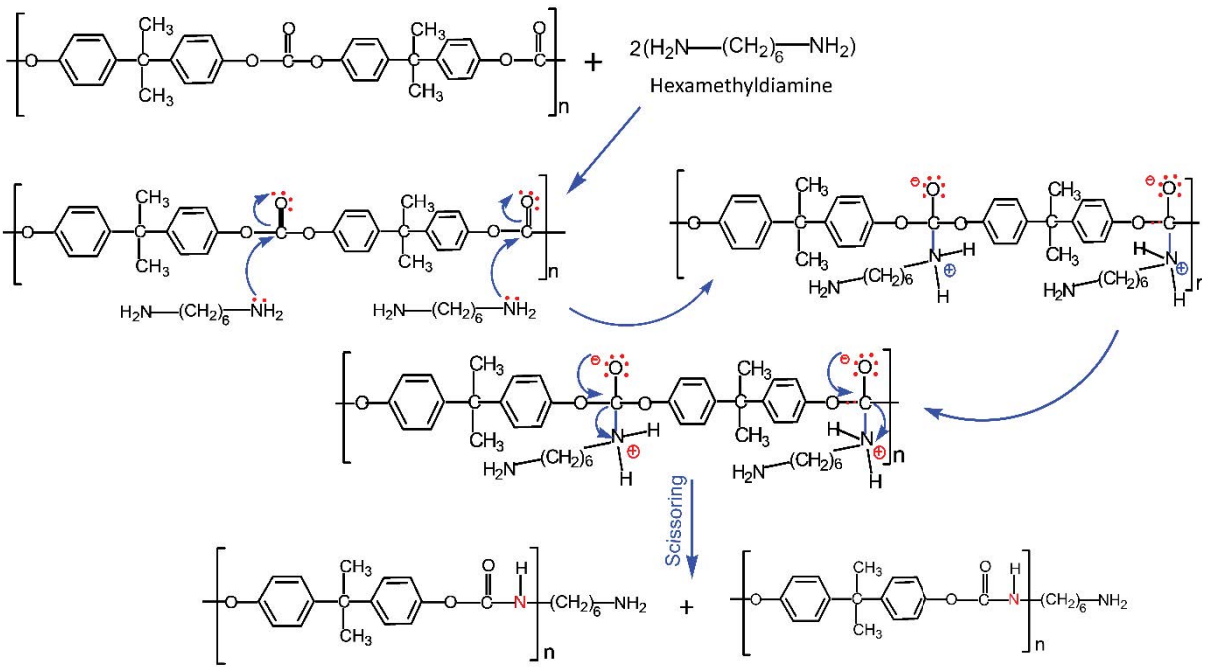

Fig. 1. Schematic of amination reaction of RPC and HMDA.

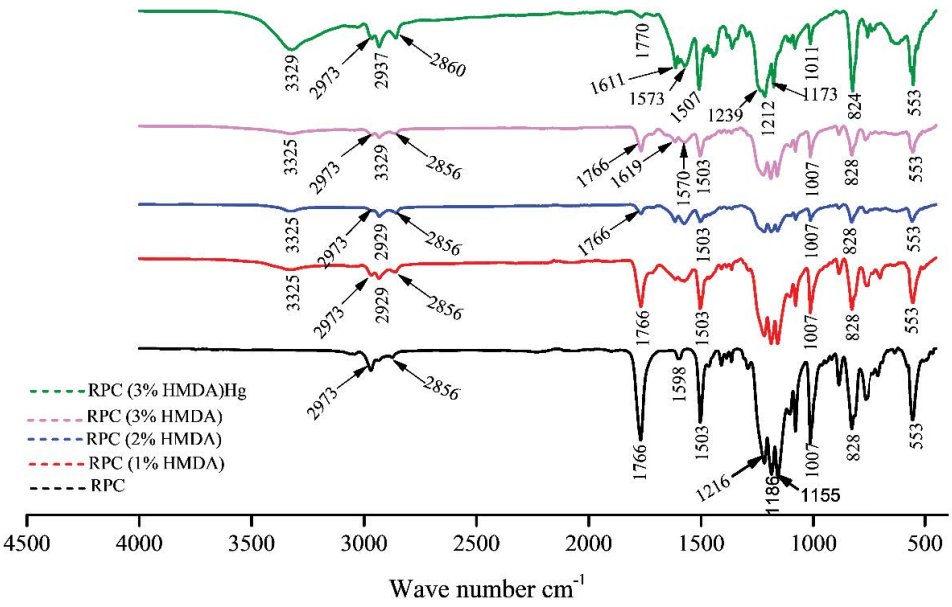

Fig. 2. FTIR spectra of RPC, ARPC with various % HMDA loadings, and ARPC 3% (HMDA)Hg.

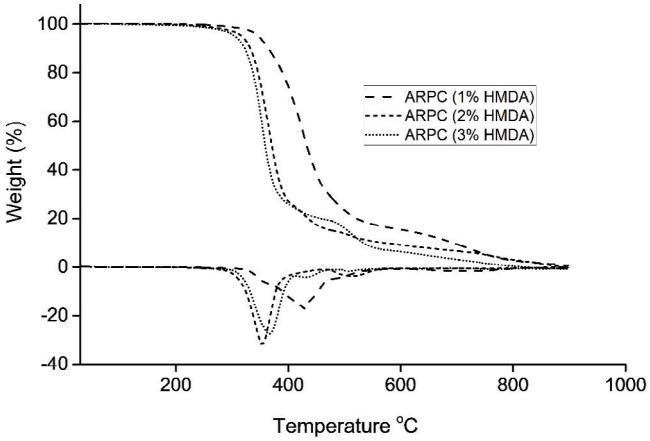

Fig. 3. TGA and DTG thermograms of ARPC.

only. Based on the data, the content of nitrogen in ARPC increased from 19% to 25% when the concentration of the HMDA was adjusted from 1% to 3%. The highest amination rate achieved under the current experiment setting was with 3% HDMA. Table S2 indicates the presence of Hg on the spent adsorbent surface which implied the adherence of Hg(II) ions onto the ARPC surface.

From the N_2 adsorption/desorption isotherms, the calculated BET surface area of ARPC was 3.81 ± 0.17 $m^2\ g^{-1}$; this is higher than that of the unmodified RPC [23]. Compared to other reported adsorbents [20], ARPC depicted a considerably high specific surface area indicating its potential as a good adsorbent for Hg(II) ions.

3.2. Response surface modeling

In line with the designed experiments, the second-order polynomial function about the removal efficiency and the three controlled variables is presented in Eq. (5):

$$\hat{y} = 56.49 - 20.93X_1 + 12.66X_2 + 3.05X_3 + 8.12X_1X_2 + 0.42X_1X_3 - 2.01X_2X_3 + 7.66X_1^2 + 4.46X_2^2 + 14.24X_3^2 \quad (5)$$

where $\hat{y}$ is the predicted percentage of Hg(II) ions removal; X_1, X_2, and X_3 are the initial Hg(II) ions concentration, pH, and initial contact time in the coded unit. The ANOVA results (Table S3) reveals a relatively large *F*-ratio of 5.85 ($P \approx 0.03$), which signify the capability of the above model in addressing the response variation; at the same time, the potential in representing the actual relationship between those independent variables and the response [22]. Briefly, the model managed to explain about 91% of the response ($R^2 \approx 0.913$) variability with an RMSE of 10.7. According to Alslaibi et al. [36], the closer the R^2 value to unity and the smaller the RMSE, the more accurate the predicted response, which indicated that the model performance is reasonable. Moreover, the lack of fit with a small *F*-ratio of 1.15 ($P \approx 0.50$) shows it is insignificant, suggesting further the model's validity [37]. Considering maximizing the percentage of Hg(II) ions removal, the following operating conditions are derived: from the model: initial Hg(II) ions concentration of 1 mg L^{-1}, pH value of 7, and contact time of 10 min where the predicted removal efficiency was almost 100%.

3.3. Effect of initial Hg(II) ions concentration

Based on the regression report (Table 2), the efficiency of adsorption removal depends strongly on the initial concentration of ARPC. They have an inverse relationship as indicated by the negative regression coefficient (b_1). In this regard, the removal efficiency is higher when the IC is at a low level due to the availability of adequate binding sites on the ARPC; whereas at a higher IC level, along with the increase in the number of mole of Hg(II) ions, there is a resultant decrease in the number of free binding sites due to saturation [18]. Such a trend has been reported in a previous

study regarding the effect of the initial concentration of metal ions on other sorbent materials [27].

3.4. Effect of pH

The pH of the solution affects the adsorbent surface charge, adsorbate ionization, and thus the adsorption process. The efficiency of adsorption removal of Hg(II) ions by ARPC was significantly affected by the pH value (Table 2). The removal efficiency was increased as the solution pH increased from 3 to 8. Basically, at pH 4 and below, the Hg(II) appears predominantly in the form of Hg(II) ions and $Hg(OH)^+$ [38]. These mercury species, together with H^+, compete for the active sites on the adsorbent leading to the lower removal efficiency. However, at higher pH values, $Hg(OH)_2$ is the predominant species. The neutral species does not precipitate in solution, hence interacts favorably with the ARPC leading to higher removal efficiency as observed [39].

3.5. Effect of contact time

In any adsorption process, contact time is always a crucial factor to be considered. Although the main effect of CT is insignificant ($P \approx 0.46$) within the experimental domain, however, under the current study, its quadratic effect could be significant ($P \approx 0.05$) (Table 2). By referring to the kinetic data, the removal efficiency of Hg(II) ions was observed to be high at the initial stage but slowed down as the equilibrium being approached. The rapid increase in the percent Hg(II) ions removal at the initial stage could be related to the availability of active sites on the ARPC surface. With extended contact time, however, the adsorption sites gradually became saturated [12,38]. After attaining equilibrium, a slight rise in the percent removal was also noticed with increased contact time. Such observation might be due to intraparticle diffusion, as suggested in other studies [27].

3.6. Interaction between Hg(II) ions concentration and pH

The relationship between the two factors (IC and pH) and the removal efficiency is presented in Fig. 4a. The surface plot shows that the impact of IC and pH are not much interdependent, and a high removal efficiency can be achieved around pH 7–8 at IC of 1 mg L^{-1}. Increasing pH increased the Hg(II) removal efficiency. The removal efficiency was found to decrease as IC increased; this observation was more apparent in acidic solutions. Under such circumstances, H^+, Hg(II), and $Hg(OH)^+$ contested for the available active sites on a fixed mass of ARPC, leading to possible saturation. When the active sites became saturated, further adsorption became difficult. This trend was similarly reported by other researchers [26].

Table 2
Regression analysis

Terms	Estimate	Standard error	*t*-ratio	$P > \|t\|$
b_0 (Intercept)	56.49	6.20	9.10	<0.0003*
b_1 (IC)	–20.93	3.80	–5.51	0.0027*
b_2 (pH)	12.66	3.80	3.33	0.0207*
b_3 (CT)	3.048	3.80	0.80	0.4589
b_{12} (IC × pH)	8.12	5.37	1.51	0.1914
b_{13} (IC × CT)	0.42	5.37	0.08	0.9411
b_{23} (pH × CT)	–2.01	5.37	–0.37	0.7234
b_{11} (IC × IC)	7.66	5.60	1.37	0.2291
b_{22} (pH × pH)	4.46	5.60	0.80	0.4618
b_{33} (CT × CT)	14.24	5.60	2.55	0.0515

*Statistically significant at the level of 0.05

3.7. Interaction between Hg(II) ions concentration and contact time

The effects of IC and CT on the efficiency of adsorption removal by ARPC are illustrated in Fig. 4b. It was observed that at IC of 1 mg L^{-1}, almost 99% of the Hg(II) ions were successfully removed within 10 min. However, the removal efficiency rapidly reduced when the IC increased regardless of the setting of CT. The above observations clearly outline that the two-way interaction between IC and CT is not significant at all. In general, the observed higher Hg(II) removal efficiency at the lower level of IC was attributed to the accessibility of more vacant sites, which created a strong concentration gradient between the Hg(II) ions in solution and those on the ARPC [40]. This strong concentration gradient promoted fast diffusion of Hg(II) ions into the intraparticle matrix enabling the ARPC to reach rapid equilibrium. Despite extending the CT, the lower removal efficiency with increasing IC suggested the exhaustion of the active sites, and hence, a slowed adsorption removal Hg (II) phase. This result hinted at the possibility of monolayer adsorption coverage.

3.8. Interaction between pH and contact time

As shown in Fig. 4c, the effects of pH and CT do not depend on each other. In other words, no significant interaction between pH and CT; the trend of Hg(II) removal efficiency as a function of pH is consistent throughout the CT range. When keeping the IC at 5.5 mg L^{-1}, the graph depicts an increase in the removal efficiency as the increase of solution pH. According to Iqbal et al. [27] pH affects the type and species of Hg(II) ions in solution and the adsorbent surface charge. Consequently, it impacts the sorbate–sorbent interaction.

3.9. Equilibrium adsorption studies

The adsorption isotherm is widely used to describe the concept that governs the interaction between the adsorbate and the adsorbent in an aqueous solution under stipulated conditions. The adsorption equilibria were examined using three adsorption models, that is, the Langmuir, Freundlich, and Temkin relationships. The parameters derived by fitting the three isotherm models (Fig. 5a–c) are presented in Table 3.

3.9.1. Langmuir isotherm model

The Langmuir isotherm describes the monolayer deposition of the adsorbate on the homogeneous adsorbent surface with equivalent adsorptive sites [40]. According to this

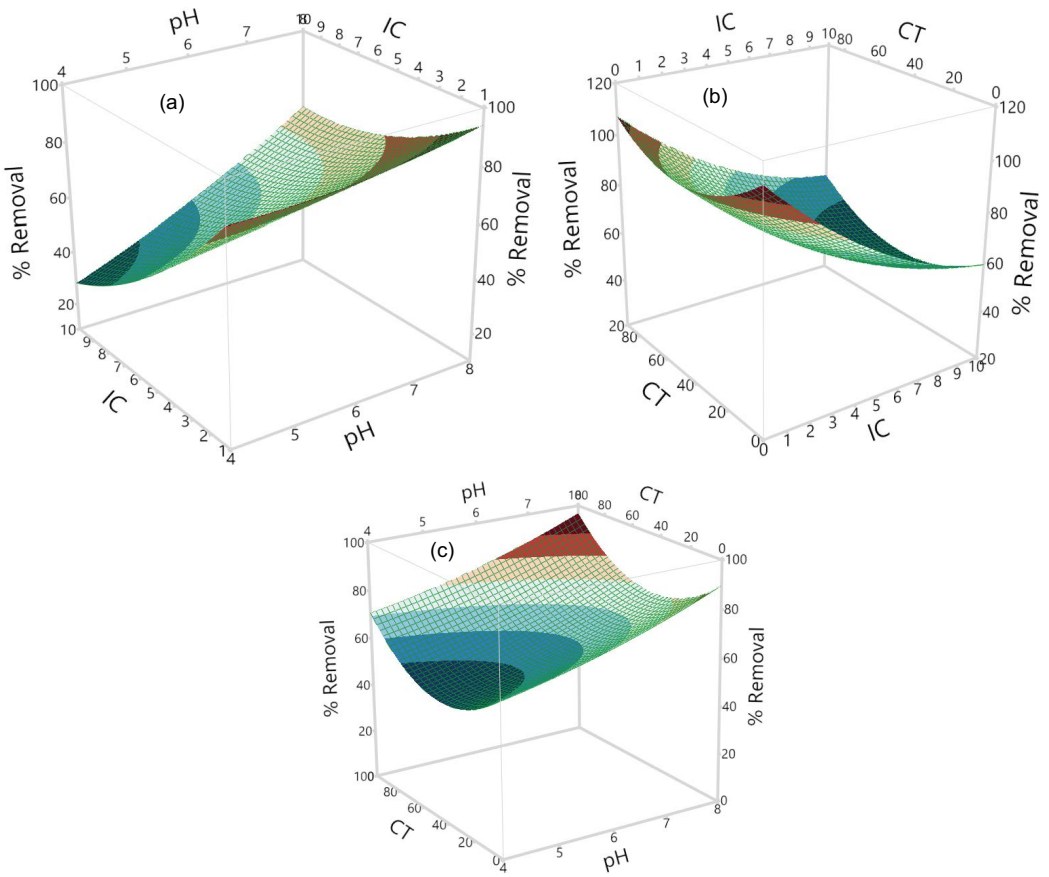

Fig. 4. Interactive effect of process variables on % Hg(II) ions removal efficiency: (a) initial Hg(II) ions concentration and pH, (b) contact time and pH, and (c) initial Hg(II) ions concentration and pH.

model, increasing the Hg(II) ions concentration will increase the Q_e until the equilibrium is established, after which, the adsorption sites become saturated. The linear expression of Langmuir isotherm is represented in Eq. (6):

$$\frac{C_e}{Q_e} = \frac{C_e}{Q_m} + \frac{1}{Q_m K_L} \tag{6}$$

where C_e is the equilibrium concentration of Hg(II) ions; Q_m is the maximum adsorption capacity; and K_L is the net adsorption enthalpy. Fig. 5a shows the Langmuir isotherm fitting of Hg(II) ions adsorption data, and the value of related parameters are listed in Table 3. Based on the Langmuir separation factor calculated using Eq. (7):

$$R_L = \frac{1}{1 + K_L C_0} \tag{7}$$

The value of $0 < R_L < 1$ (Table 3), the adsorption process was deemed as a favorable.

3.9.2. Freundlich isotherm model

The Freundlich isotherm model describes a multilayer, heterogeneous adsorption on the adsorbent surface. The model is represented by Eq. (8):

$$\log Q_e = \log K_f + \frac{1}{n} \log C_e \tag{8}$$

where K_f and n are the Freundlich constants related to the adsorption capacity and adsorption intensity, respectively. According to the result, Fig. 5b, the R^2 for the Freundlich model is slightly better as compared to the Langmuir isotherm (Table 3).

3.9.3. Temkin isotherm model

In addition, the Temkin adsorption isotherm model was also used to reflect the interaction between the Hg(II) ions and the ARPC. The Temkin model assumes that the adsorption energy declines linearly with the increase in coverage of the adsorbent surface by adsorbate, as represented by Eq. (9):

$$Q_e = \frac{RT}{b_T} \ln K_T + \frac{RT}{b_T} \ln C_e \tag{9}$$

where b_T is the Temkin constant, which is related to the adsorption energy (kJ mol^{-1}), K_T represents the equilibrium binding constant which corresponds to the maximum binding energy (L g^{-1}), T stands for the absolute temperature (K), and R is the gas constant (8.314 × 10^{-3} kJ mol^{-1} K^{-1}) [41].

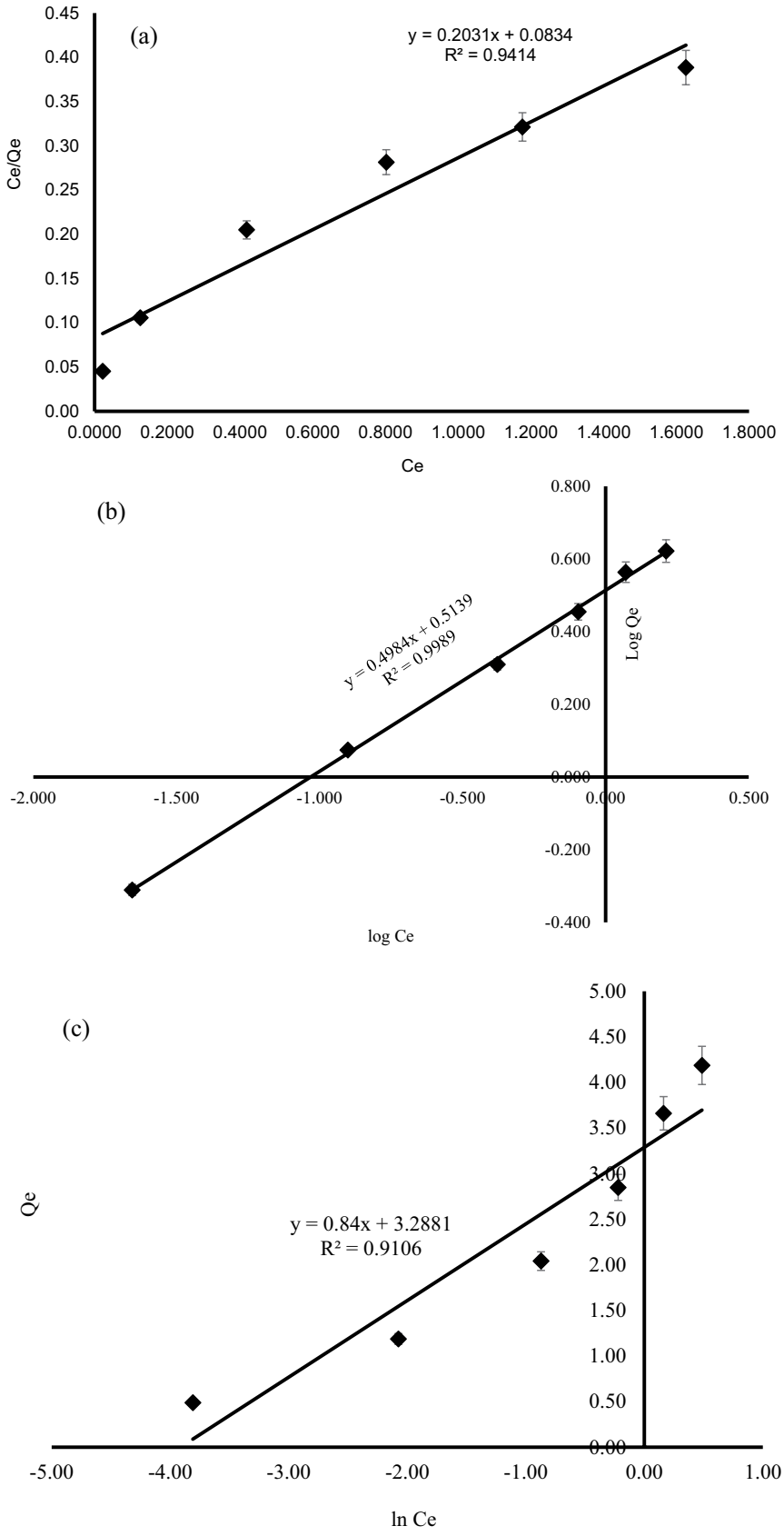

Fig. 5. Adsorption isotherm model: (a) Langmuir model, (b) Freundlich model, and (c) Temkin model for Hg(II) ions adsorption on ARPC.

The Temkin constants b_T and K_T were obtained from the slope and intercept of a plot of Q_e vs. lnC_e (Fig. 5c) and the numerical values are given in Table 3. From the result, the equilibrium-binding constant K_T was equal to 26.79 L g^{-1}, which reflects the maximum binding energy [41]. Based on the regression coefficient ($R^2 \approx 0.9106$), the Temkin model does not fit the experimental data well.

3.10. Adsorption mechanism

The improved Hg(II) ions removal efficiency of APRC as compared to RPC has demonstrated the effect of surface modification; which clueing the involvement of the incorporated amine functionality in the adsorption mechanism. In this context, the adsorption of Hg(II) onto the ARPC surface is plausibly the interaction between the nitrogen of the amine group and the Hg(II) ions. In general, the lone pair electrons of nitrogen atoms can be donated to the coordination bonds between nitrogen and metal cations, including Hg(II) [7,42]. The proposed interaction scheme between the Hg(II) and the ARPC is shown in Fig. 6.

The performance of ARPC for the removal of Hg(II) ions was compared with other adsorbents reported in the literature. The results displayed in Table 4 indicated that ARPC exhibits higher adsorption capacity compared to the coconut-based adsorbents [44,45]. Similarly, the aminated product demonstrated much higher Hg(II) ion removal capability over the nitrated polycarbonate [23]; which is attributed to the enhanced chelation behavior of the amine functionality. Hence, the waste-derived aminated product seems to be a promising low-cost adsorbent for Hg(II) remediation of aqueous media.

3.11. Adsorption kinetics studies

The adsorption kinetics reflect the mechanism of the adsorption process [32]. The experimental kinetic data were fitted to PFO and PSO kinetic models. The PFO kinetic model is represented by Eq. (10):

$$\log\left(Q_e - Q_t\right) = \log Q_e + \frac{k_1}{2.303}t \tag{10}$$

where Q_e and Q_t (mg g^{-1}) are the amount (Hg(II) ions) adsorbed at equilibrium and time t, respectively and k_1 represents the PFO rate constant (min^{-1}). The PFO kinetic parameters, including Q_e and k_1 were estimated from Fig. 7a. The PFO kinetic model assumes that the sorption of the adsorbate onto the adsorbent involves physical bonding.

The experimental data were also fitted to the PSO kinetic model that describes the adsorbate interacts with adsorbent through the chemisorption process. Eq. (11) represents the PSO kinetic model:

$$\frac{t}{Q_t} = \frac{t}{Q_e} + \frac{1}{k_2\left(Q_e\right)^2} \tag{11}$$

where k_2 (g mg^{-1} min^{-1}) is the PSO rate constant, which was calculated from the intercept of t/Q_t vs. t plot (Fig. 7b). Comparing the correlation coefficients (R^2), the PSO model was the best to describe the kinetics of the Hg(II) ions sorption onto the ARPC since it shows a higher R^2 value than the PFO model. It can be concluded that the adsorption

Table 4
Comparison of adsorption capacities of different adsorbents on Hg(II) ions

Adsorbents	Q_m (mg g^{-1})	K_f (mg g^{-1})	References
Coconut activated carbon	5.2	3.352	[43]
Coconut fiber char	1.991	–	[44]
Coconut pit char	3.142	–	[44]
Nitrated polycarbonate	0.289	0.261	[23]
ARPC	4.924	3.365	This study

Table 3
Langmuir, Freundlich, and Temkin isotherm parameters for the adsorption of Hg(II) ions

Langmuir			Freundlich			Temkin		
R^2	Q_m (mg g^{-1})	R_L	R^2	n	K_f (mg g^{-1})	R^2	b_T (kJ mol^{-1})	K_T (L g^{-1})
0.9414	4.92	0.04	0.9989	2.01	3.37	0.9106	0.84	26.79

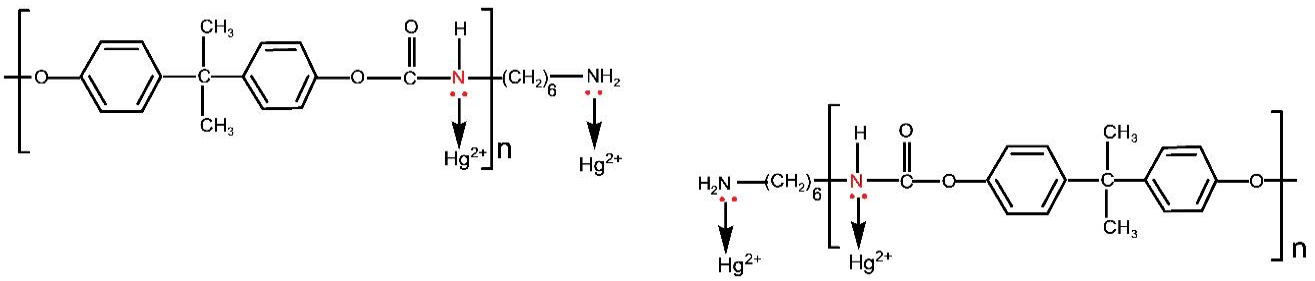

Fig. 6. A suggested mechanism for the removal of Hg(II) by the ARPC.

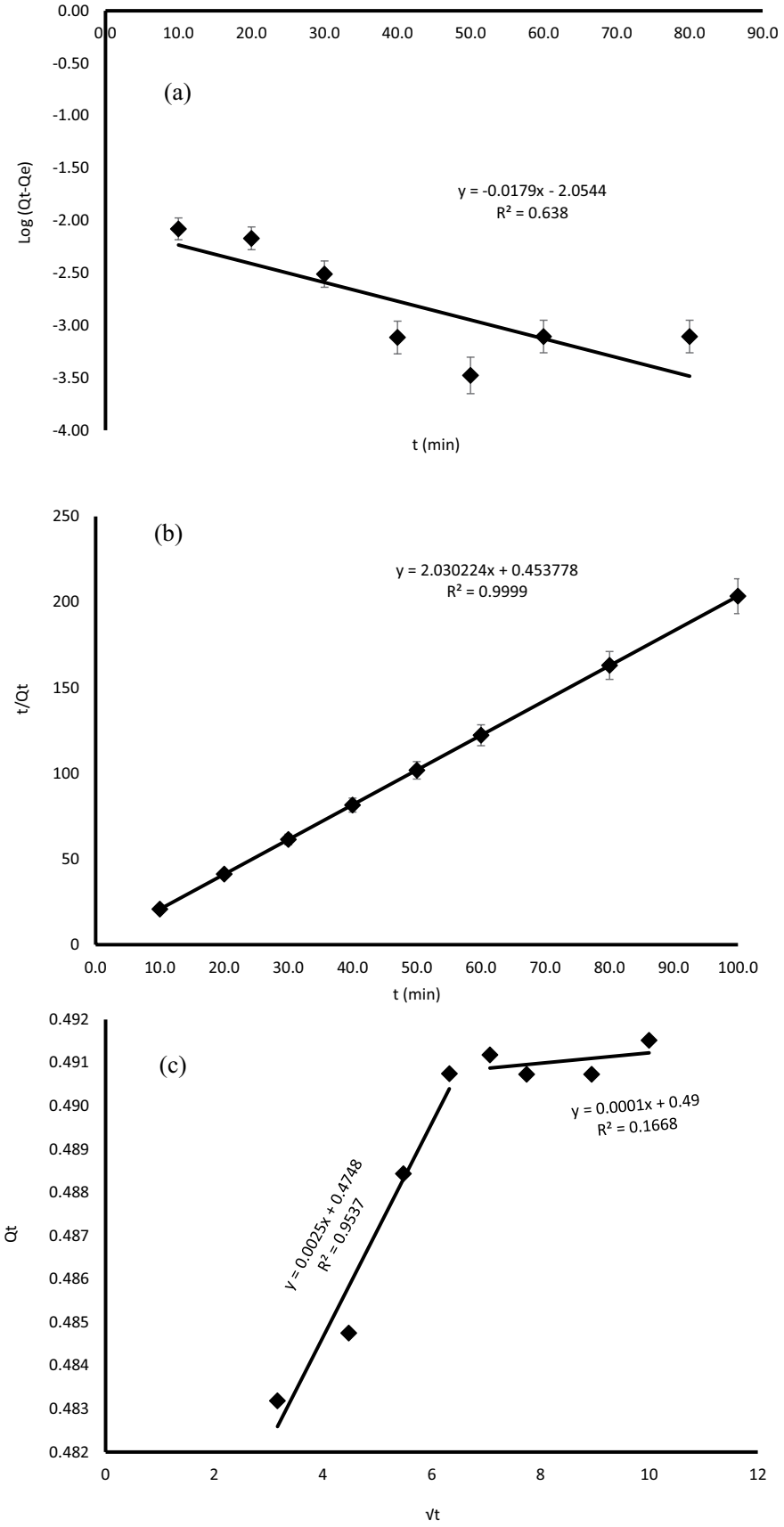

Fig. 7. (a) Pseudo-first-order, (b) pseudo-second-order, and (c) intra-particle diffusion models for the removal of Hg(II) ions from aqueous medium.

of Hg(II) ions in this study involved the chemisorption process.

3.12. Intraparticle diffusion kinetic models

The intraparticle diffusion model was applied to determine the adsorption behavior of Hg(II) ions on the ARPC. The intraparticle model is represented as follows:

$$Q_t = k_{ip}\sqrt{t} + C \tag{12}$$

where, k_{ip} (mg g^{-1} min$^{-0.5}$) represents the intraparticle diffusion constant, and C is the effect of the boundary layer. The plot of Q_t vs. $\sqrt{t}$ (Fig. 7c) revealed two linear portions; the first sharp slope phase might represent the macropore and mesopore diffusion, while the second phase probably represents micropore diffusion due to the porous nature of the ARPC. Again, the slower second slope suggested that intraparticle diffusion is not involved in the adsorption. A similar observation was made by other researchers [40]. The adsorption mechanism proceeds by initial mass transfer of Hg(II) ions species into the macropore, mesopore, and micropore of ARPC and reaching the active sites. This diffusion is followed by the chemisorption via electron pair sharing between the Hg(II) ions species and the oxygen and nitrogen on the ARPC, as illustrated in Fig. 6 in the previous section.

3.13. Desorption and reusability

The reusability of ARPC in four consecutive adsorption–desorption cycles is presented in Fig. 8. It is clearly seen that the removal efficiency was gradually decreased after each subsequent cycle. This observation might be attributed to the exhaustion of some active sites on the spent adsorbent. This observation agrees with the reports from other related studies [45]. It can be concluded that the ARPC depicted reasonable reusability capacity after regeneration and can possibly be used repetitively and efficiently as an economic adsorbent for the removal of Hg(II) ions from an aqueous medium.

3.14. Application of the ARPC in real water samples

Natural water may contain different matrices that may interfere with the Hg(II) ions removal process due to competition for the active sites on the adsorbent. To examine the performance of ARPC in the removal of Hg(II) ions in real water samples, five different water samples including UPW, TW, LW, MW, and DW, were spiked with 1 mg L^{-1} of Hg(II) ions and subjected to adsorption process under optimum settings. The results presented in Fig. 9 demonstrate around 97% to 99% removal efficiencies were achieved considering different water samples. This implies that the adsorbent is not affected much by the matrix effect of aqueous samples, therefore, it is a reasonable adsorbent candidate for wastewater remediation.

4. Conclusions

The results from this study have shown that the chemically modified RPC derived from the CD/DVD waste had the potential to remove Hg(II) ions in an aqueous solution. With BBD and RSM, the optimum condition for the removal of Hg(II) ions was found as IC of 1 mg L^{-1}, pH 7, and CT of 10 min. On the basis of the higher regression coefficient value ($R^2 \approx 0.9989$) from the Freundlich batch equilibrium adsorption experiments, the adsorption process of Hg(II) ions on ARPC fitted the Freundlich isotherm model. The kinetic data best fitted the PSO rate equation as observed from the regression coefficients ($R^2 = 0.9999$). The test results on real water samples, using the waste-derived adsorbent showed high Hg(II) ions removal efficiency on various water samples, which suggests that the material was not affected by matrix interference. Furthermore, the ARPC showed high potential to be reused repeatedly for a number of adsorption–desorption cycles. So on the basis

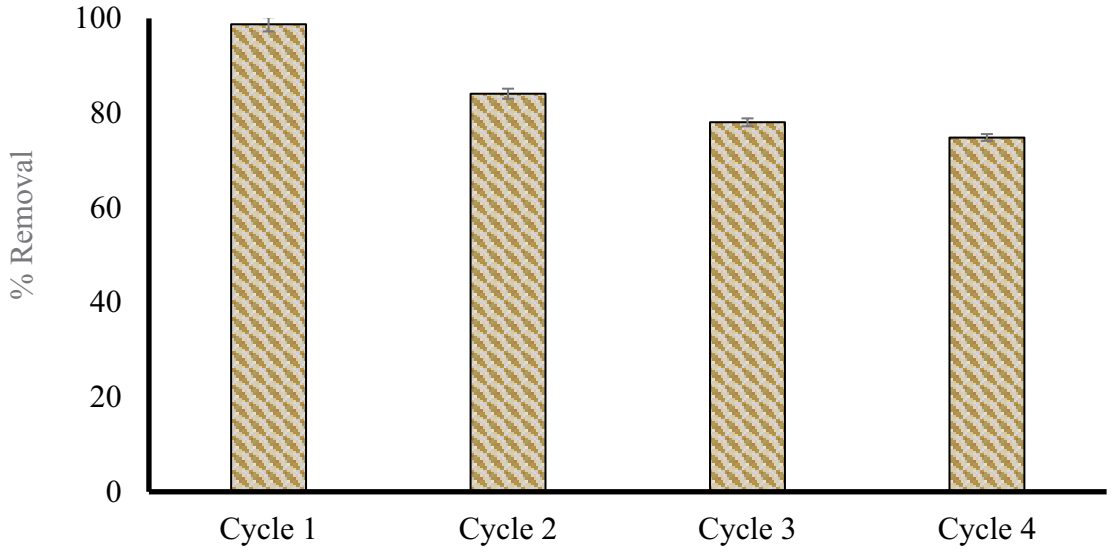

Fig. 8. Adsorption–desorption cycles of Hg(II) ions on ARPC using 0.75 M thiourea in 2% HCl (under optimum settings).

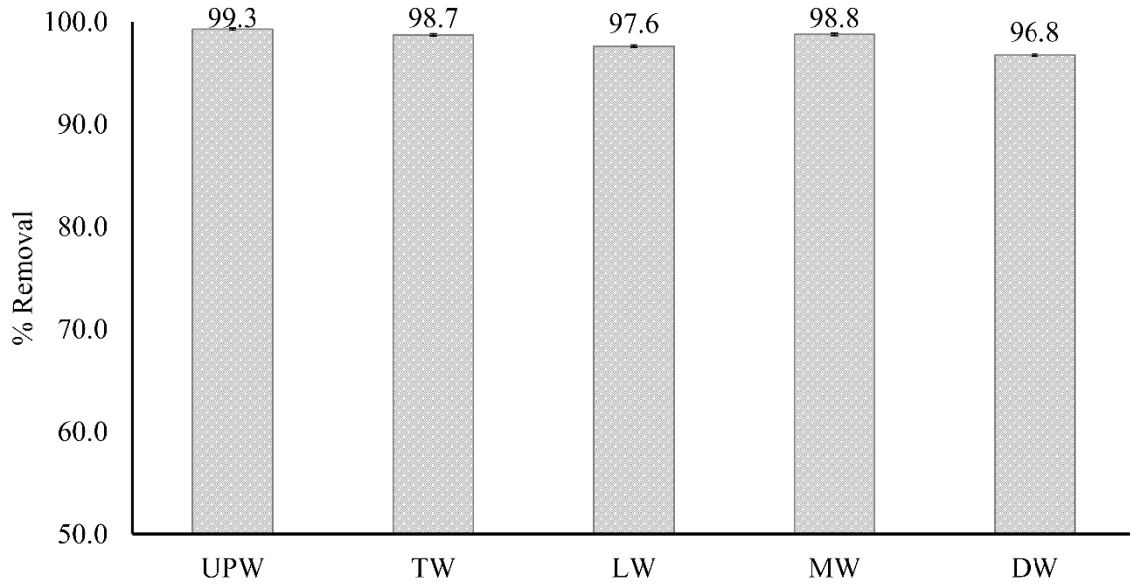

Fig. 9. Removal efficiency of Hg(II) ions by ARPC from real water samples (under optimum settings).

of these experimental findings, it may be concluded that ARPC is suitable, economical, and effective for the removal of Hg(II) ions from aqueous media. It can therefore serve as a potential alternative to the more expensive conventional adsorbents. Thanks to the introduction of reactive amine, ARPC is therefore highly susceptible for further modification in order to serve corresponding application purposes.

Acknowledgments

This work was supported financially by the Ministry of Higher Education Malaysia (Fundamental Research Grant Scheme: FP074-2018A).

References

[1] G. Kaur, S. Pavia, Physical properties and microstructure of plastic aggregate mortars made with acrylonitrile-butadiene-styrene (ABS), polycarbonate (PC), polyoxymethylene (POM) and ABS/PC blend waste, J. Build. Eng., 31 (2020) 101341, doi: 10.1016/j.jobe.2020.101341.

[2] M.A.P. Rojas, M.J.M. Conde, F.P. Gálvez, P.R.D. Hita, Reuse of CD and DVD wastes as reinforcement in gypsum plaster plates, Materials, 13 (2020) 989, doi: 10.3390/ma13040989.

[3] R. Rajarao, I. Mansuri, R. Dhunna, R. Khanna, V. Sahajwalla, Characterisation of gas evolution and char structural change during pyrolysis of waste CDs, J. Anal. Appl. Pyrolysis, 105 (2014) 14–22.

[4] Z. Noorimotlagh, S.A. Mirzaee, S.S. Martinez, S. Alavi, M. Ahmadi, N. Jaafarzadeh, Adsorption of textile dye in activated carbons prepared from DVD and CD wastes modified with multi-wall carbon nanotubes: equilibrium isotherms, kinetics and thermodynamic study, Chem. Eng. Res. Des., 141 (2019) 290–301.

[5] R. Rajarao, I. Mansuri, R. Dhunna, R. Khanna, V. Sahajwalla, Study of structural evolution of chars during rapid pyrolysis of waste CDs at different temperatures, Fuel, 134 (2014) 17–25.

[6] S. Singh, Y. Lei, A. Schober, Direct extraction of carbonyl from waste polycarbonate with amines under environmentally friendly conditions: scope of waste polycarbonate as a carbonylating agent in organic synthesis, RSC Adv., 5 (2015) 3454–3460.

[7] H. Albatrni, H. Qiblawey, M.H.E. Naas, Comparative study between adsorption and membrane technologies for the removal of mercury, Sep. Purif. Technol., 257 (2021) 117833, doi: 10.1016/j.seppur.2020.117833.

[8] H. Zhang, S. Pap, M.A. Taggart, K.G. Boyd, N.A. James, S.W. Gibb, A review of the potential utilisation of plastic waste as adsorbent for removal of hazardous priority contaminants from aqueous environments, Environ. Pollut., 258 (2020) 113698, doi: 10.1016/j.envpol.2019.113698.

[9] A. Ahmad, J.A. Siddique, M.A. Laskar, R. Kumar, S.H.M. Setapar, A. Khatoon, R.A. Shiekh, New generation Amberlite XAD resin for the removal of metal ions: a review, J. Environ. Sci., 31 (2015) 104–123.

[10] J. Choma, M. Marszewski, L. Osuchowski, J. Jagiello, A. Dziura, M. Jaroniec, Adsorption properties of activated carbons prepared from waste CDs and DVDs, ACS Sustainable Chem. Eng., 3 (2015) 733–742.

[11] S.M. Albukhari, M.A. Hussein, M.A.A. Rahman, H.M. Marwani, Highly selective heteroaromatic sulfur containing polyamides for Hg^{+2} environmental remediation, Des. Monomers Polym., 23 (2020) 25–39.

[12] M. Naushad, Surfactant assisted nano-composite cation exchanger: development, characterization and applications for the removal of toxic Pb^{2+} from aqueous medium, Chem. Eng. J., 235 (2014) 100–108.

[13] E. Ghasemi, A. Heydari, M. Sillanpää, Superparamagnetic Fe_3O_4@ EDTA nanoparticles as an efficient adsorbent for simultaneous removal of Ag(I), Hg(II), Mn(II), Zn(II), Pb(II) and Cd(II) from water and soil environmental samples, Microchem. J., 131 (2017) 51–56.

[14] G. Sharma, A. Kumar, M. Naushad, A. Kumar, H. Ala'a, P. Dhiman, A.A. Ghfar, F.J. Stadler, M. Khan, Photoremediation of toxic dye from aqueous environment using monometallic and bimetallic quantum dots based nanocomposites, J. Cleaner Prod., 172 (2018) 2919–2930.

[15] M. Naushad, Z.A. Al-Othman, Separation of toxic Pb^{2+} metal from aqueous solution using strongly acidic cation-exchange resin: analytical applications for the removal of metal ions from pharmaceutical formulation, Desal. Water Treat., 53 (2015) 2158–2166.

[16] G. Sharma, D. Pathania, M. Naushad, N. Kothiyal, Fabrication, characterization and antimicrobial activity of polyaniline Th(IV) tungstomolybdophosphate nanocomposite material: efficient removal of toxic metal ions from water, Chem. Eng. J., 251 (2014) 413–421.

[17] S.W. Khor, Y.K. Lee, M.R.B. Abas, K.S. Tay, Application of chalcone-based dithiocarbamate derivative incorporated sol–gel for the removal of Hg(II) ion from water, J. Sol-Gel Sci. Technol., 82 (2017) 834–845.
[18] M. Kumar, A.K. Singh, M. Sikandar, Biosorption of Hg(II) from aqueous solution using algal biomass: kinetics and isotherm studies, Heliyon, 6 (2020) e03321, doi: 10.1016/j.heliyon.2020.e03321.
[19] E. Khanniri, M. Yousefi, A.M. Mortazavian, N. Khorshidian, S. Sohrabvandi, M. Arab, M.R. Koushki, Effective removal of lead(II) using chitosan and microbial adsorbents: response surface methodology (RSM), Int. J. Biol. Macromol., 178 (2021) 53–62.
[20] M.E. Mahmoud, A.E. Abdou, S.B. Ahmed, Conversion of waste styrofoam into engineered adsorbents for efficient removal of cadmium, lead and mercury from water, ACS Sustainable Chem. Eng., 4 (2016) 819–827.
[21] T. Sahan, F. Erol, S. Yilmaz, Mercury(II) adsorption by a novel adsorbent mercapto-modified bentonite using ICP-OES and use of response surface methodology for optimization, Microchem. J., 138 (2018) 360–368.
[22] A. Alipour, S. Zarinabadi, A. Azimi, M. Mirzaei, Adsorptive removal of Pb(II) ions from aqueous solutions by thiourea-functionalized magnetic ZnO/nanocellulose composite: optimization by response surface methodology (RSM), Int. J. Biol. Macromol., 151 (2020) 124–135.
[23] S.A. Abdallah, K.S. Tay, K.H. Low, Feasibility of mercury(II) ion removal by nitrated polycarbonate derived from waste optical discs, Int. J. Environ. Sci. Technol., 17 (2020) 4161–4170.
[24] V.V. Delinder, D.R. Wheeler, L.J. Small, M.T. Brumbach, E.D. Spoerke, I. Henderson, G.D. Bachand, Simple, benign, aqueous-based amination of polycarbonate surfaces, ACS Appl. Mater. Interfaces, 7 (2015) 5643–5649.
[25] N. Saranya, E. Nakeeran, G. Nandagopal, N. Selvaraju, Optimization of adsorption process parameters by response surface methodology for hexavalent chromium removal from aqueous solutions using *Annona reticulata* Linn peel microparticles, Water Sci. Technol., 75 (2017) 2094–2107.
[26] N.D. Mu'azu, S.A. Haladu, N. Jarrah, M. Zubair, M.H. Essa, S.A. Ali, Polyaspartate extraction of cadmium ions from contaminated soil: evaluation and optimization using central composite design, J. Hazard. Mater., 342 (2018) 58–68.
[27] M. Iqbal, Z. Ali, M.A. Qamar, A. Ali, F. Hussain, M. Abbas, J. Nisar, Nickel adsorption onto polyurethane ethylene and vinyl acetate sorbents, Water Sci. Technol., 76 (2017) 219–235.
[28] M. Alimohammadi, Z. Saeedi, B. Akbarpour, H. Rasoulzadeh, K. Yetilmezsoy, M.A. Al-Ghouti, M. Khraisheh, G. McKay, Adsorptive removal of arsenic and mercury from aqueous solutions by eucalyptus leaves, Water Air Soil Pollut., 228 (2017) 429, doi: 10.1007/s11270-017-3607-y.
[29] X. Yao, H. Wang, Z. Ma, M. Liu, X. Zhao, D. Jia, Adsorption of Hg(II) from aqueous solution using thiourea functionalized chelating fiber, Chin. J. Chem. Eng., 24 (2016) 1344–1352.
[30] Y.J. Shi, T. Zhang, H.Q. Ren, A. Kruse, R.F. Cui, Polyethylene imine modified hydrochar adsorption for chromium(VI) and nickel(II) removal from aqueous solution, Bioresour. Technol., 247 (2018) 370–379.
[31] G. Sharma, M. Naushad, Adsorptive removal of noxious cadmium ions from aqueous medium using activated carbon/zirconium oxide composite: isotherm and kinetic modelling, J. Mol. Liq., 310 (2020) 113025, doi: 10.1016/j.molliq.2020.113025.
[32] T.A. Saleh, Isotherm, kinetic, and thermodynamic studies on Hg(II) adsorption from aqueous solution by silica-multiwall carbon nanotubes, Environ. Sci. Pollut. Res., 22 (2015) 16721–16731.
[33] R. Farzana, R. Rajarao, B.R. Bhat, V. Sahajwalla, Performance of an activated carbon supercapacitor electrode synthesised from waste Compact Discs (CDs), J. Ind. Eng. Chem., 65 (2018) 387–396.
[34] C. Larosa, N. Patra, M. Salerno, L. Mikac, R.M. Meri, M. Ivanda, Preparation and characterization of polycarbonate/multiwalled carbon nanotube nanocomposites, Beilstein J. Nanotechnol., 8 (2017) 2026–2031.
[35] C. Zimmerer, L. Ziegler, G. Heinrich, G. Steiner, Time resolved characterization of the solid-state reaction between polycarbonate and primary amine, Eur. Polym. J., 98 (2018) 313–320.
[36] T.M. Alslaibi, I. Abustan, M.A. Ahmad, A.A. Foul, Application of response surface methodology (RSM) for optimization of Cu^{2+}, Cd^{2+}, Ni^{2+}, Pb^{2+}, Fe^{2+}, and Zn^{2+} removal from aqueous solution using microwaved olive stone activated carbon, J. Chem. Technol. Biotechnol., 88 (2013) 2141–2151.
[37] W. Yuan, J. Cheng, H. Huang, S. Xiong, J. Gao, J. Zhang, S. Feng, Optimization of cadmium biosorption by Shewanella putrefaciens using a Box-Behnken design, Ecotox. Environ. Saf., 175 (2019) 138–147.
[38] M. Anbia, S. Amirmahmoodi, Removal of Hg(II) and Mn(II) from aqueous solution using nanoporous carbon impregnated with surfactants, Arabian J. Chem., 9 (2016) S319–S325.
[39] C. Jeon, K.L. Solis, H.R. An, Y. Hong, A.D. Igalavithana, Y.S. Ok, Sustainable removal of Hg(II) by sulfur-modified pine-needle biochar, J. Hazard. Mater., 388 (2020) 122048, doi: 10.1016/j.jhazmat.2020.122048.
[40] N.F. Ahmad, M.A. Kamboh, H.R. Nodeh, S.N.B.A. Halim, S. Mohamad, Synthesis of piperazine functionalized magnetic sporopollenin: a new organic-inorganic hybrid material for the removal of lead(II) and arsenic(III) from aqueous solution, Environ. Sci. Pollut. Res., 24 (2017) 21846–21858.
[41] M.A. Yaari, T.A. Saleh, O. Saber, Removal of mercury from polluted water by a novel composite of polymer carbon nanofiber: kinetic, isotherm, and thermodynamic studies, RSC Adv., 11 (2021) 380–389.
[42] A. Ahmad, A. Khatoon, S.H.M. Setapar, R. Kumar, M. Rafatullah, Chemically oxidized pineapple fruit peel for the biosorption of heavy metals from aqueous solutions, Desal. Water Treat., 57 (2016) 6432–6442.
[43] X. Lu, J. Jiang, K. Sun, J. Wang, Y. Zhang, Influence of the pore structure and surface chemical properties of activated carbon on the adsorption of mercury from aqueous solutions, Mar. Pollut. Bull., 78 (2014) 69–76.
[44] K. Johari, A.S. Alias, N. Saman, S.T. Song, H. Mat, Removal performance of elemental mercury by low-cost adsorbents prepared through facile methods of carbonisation and activation of coconut husk, Waste Manage. Res., 33 (2015) 81–88.
[45] S. Bao, K. Li, P. Ning, J. Peng, X. Jin, L. Tang, Highly effective removal of mercury and lead ions from wastewater by mercaptoamine-functionalised silica-coated magnetic nano-adsorbents: behaviours and mechanisms, Appl. Surf. Sci., 393 (2017) 457–466.

Supplementary information

Adsorption removal of Hg(II) ion by waste-derived aminated polycarbonate

Table S1
Experimental runs based on the BBD

No	Pattern	Initial Hg^{2+} concentration (mg L^{-1}) (x_1)	pH (x_2)	Contact time (min) (x_3)	% Removal	Predicted % removal
1	+ 0 +	5.5	8	90	97.19	90.90
2	+ 0 −	5.5	8	10	87.86	84.80
3	+ − 0	1.0	8	50	92.67	94.09
4	− − 0	1.0	4	50	92.92	84.99
5	0 0 0	5.5	6	50	62.55	56.49
6	0 + +	10	6	90	60.55	60.51
7	− + 0	10	4	50	28.31	26.89
8	0 0 0	5.5	6	50	44.59	56.49
9	+ + 0	10	8	50	60.52	68.45
10	0 0 0	5.5	6	50	62.33	56.49
11	0 + −	10	6	10	60.88	54.41
12	0 − +	1.0	6	90	95.07	102.37
13	− 0 +	5.5	4	90	66.54	65.57
14	− 0 −	5.5	4	10	49.16	59.48
15	0 − −	1.0	6	10	97.07	96.28

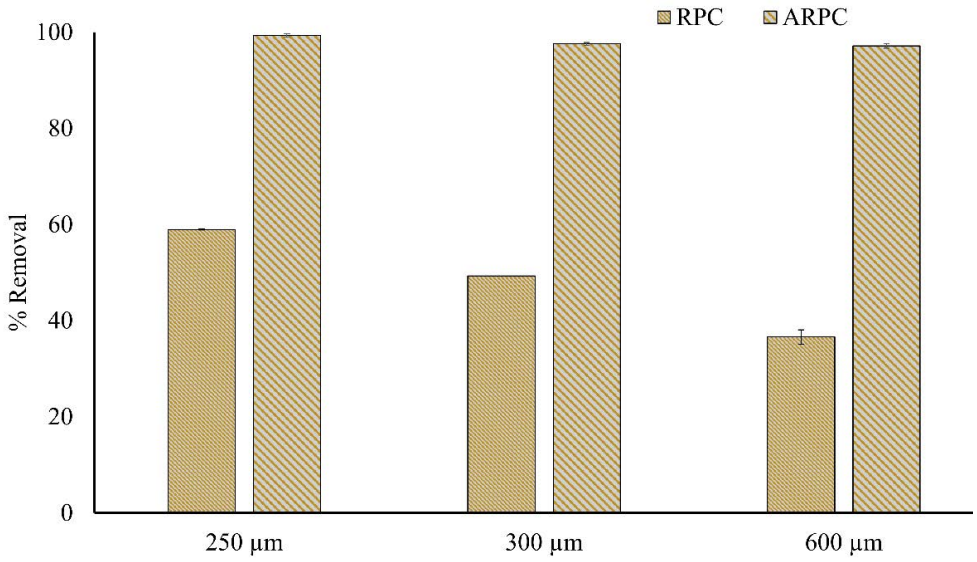

Fig. S1. Effect of particle size on removal efficiency of Hg(II) ions by RPC and ARPC (amount of adsorbents = 50 mg, IC = 1.0 mg L^{-1}, CT 24 h, pH 7.0, agitation rate = 150 rpm, the volume of solution = 25 mL, and room temperature (30°C ± 1°C).

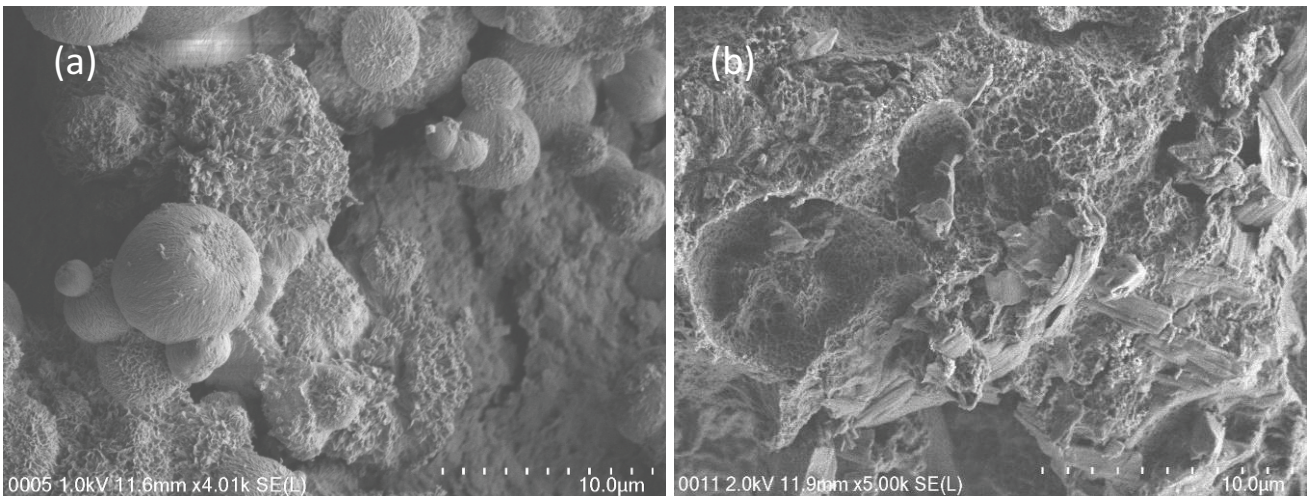

Fig. S2. FESEM micrographs of (a) RPC and (b) ARPC.

Table S2
EDS results showing elemental compositions of ARPC with various wt% HMDA treatment

Element	ARPC 1%	ARPC 2%	ARPC 3%	ARPC-Hg
Carbon (C)	66 ± 1	64 ± 2	65 ± 4	67 ± 5
Oxygen (O)	14 ± 1	15 ± 1	14 ± 2	9 ± 3
Nitrogen (N)	19 ± 1	22 ± 2	25 ± 1	24 ± 2
Hg	–	–	–	0.16 ± 0.06

Table S3
Analysis of variance

Source	DF	Sum of squares	Mean square	*F*-ratio	*P* > *F*
Model	9	6,083.58	675.95	5.85	0.0330*
Error	5	577.43	115.49		
C. total	14	6,661.00			
Lack of fit (LOF)	3	364.992	121.664	1.1454	0.4975
Pure error	2	212.439	106.220		
Total error	5	577.431			
Mean of response (%)				70.55	
R-square (*R*Sq.) (R^2)				0.913	
R-square adjusted				0.757	
Maximum *R*Sq. (R^2)				0.9681	
Root mean square error (RMSE)				10.7	

*Statistically significant at the level of 0.05.